23rd ABCM International Congress of Mechanical Engineering
December 6-11, 2015, Rio de Janeiro, RJ, Brazil

COMBINING ACOUSTIC EMISSION TECHNIQUES WITH A VERSION OF THE LATTICE DISCRETE ELEMENT METHOD FOR DAMAGE PROCESS ASSESSMENT IN HETEROGENEOUS MATERIALS

Gabriel Birck
Leonardo Renner Avila
Ignacio Iturrioz
Mechanical Engineering Department, Federal University of Rio Grande do Sul, Rua Sarmento Leite, 435, Porto Alegre, RS, 90050-170, Brazil.
gabriel.birck@ufrgs.br; leonardo.renner@ufrgs.br; ignacio@mecanica.ufrgs.br

Abstract. *In the present paper, a version of the tri-dimensional Lattice Discrete Element Method (LDEM) and Acoustic Emission (EA) technique were used to assess the damage evolution in heterogeneous materials. The LDEM method allows making a consistent calibration with the real material, maintaining an energy balance consistence. The motion equation, resultant from the spatial discretization, is integrated using an explicit scheme (finite difference method). The capability of this model to simulate the process throughout the time is also used to model the acoustic emission (AE) test. Standard results and the information obtained by mean of the AE information allow monitoring the damage evolution in the simulation. Discussions about the utility of this numerical information to complement the real AE test are finally presented.*

Keywords: *Lattice Discrete Element Method, Acoustic Emission Techniques, Heterogeneous Material.*

1. INTRODUCTION

From a physical point of view, damage phenomena consist either of surface discontinuities in the form of cracks or of volume discontinuities in the form of cavities (Lemaitre and Chaboche, 1990; Krajcinovic, 1996). Macroscopically, it's, therefore, necessary to identify internal variables that reflect the damage level in the material. The most advanced method for a non-destructive quantitative evaluation of damage progression is the Acoustic Emission (AE) technique. Physically, AE is a phenomenon caused by a structural alteration in a solid material in which transient elastic-waves, due to a rapid release of strain energy, are generated. AEs are also known as stress-wave emissions.

In the present work a version of the Discrete Element Method built by bars (LDEM) are employed. This approach pertains to the alternative set of computational methods called by Munjiza (2009), "Computational Mechanics of Discontinua" introduced during the 1960s, which is characterized by the lack of differential or integral equations to describe the model to study the space domain. In the mentioned approach, the behavior of the solid is function of the individual elements, e.g., particles or bars.

Here it's simulated compression tests of cubic specimens using different size and boundary conditions, built in quasi-fragile material. The results obtained in terms of standard results (the global stress-strain response, the energy balance and the final configurations) are presented. Also, the acceleration is registered in one point of the specimen's surface and interpreted as data provided by a real device EA. Using the standard and AE results, it is possible understand and describe better the damage process for the material and boundary condition specified.

2. ACOUSTIC EMISSION

AE waves, whose frequencies typically range from kHz to MHz, propagate through the material towards the surface of the structural element, where they can be detected by sensors which transform the strain energy packages into electrical signals. Traditionally, in AE testing, a number of parameters are recorded from the signals such as arrival time, velocity, amplitude, duration and frequency. From these parameters, damage conditions and localization of AE sources in the specimens are determined (Carpinteri *et al.*, 2009).

Using the AE technique, an effective damage assessment criterion is provided by the statistical analysis of the amplitude distribution of the acoustic emission (AE) signals generated by growing microcracks. The amplitudes of such signals are distributed according to the Gutenberg-Richter (GR) law, $N(\geq A) \propto A^{-b}$, where N is the number of AE signals with amplitude $\geq A$. The exponent b of the GR law, so-called b-value, changes with the different stages of damage growth: while the initially dominant microcracking generates a large number of low-amplitude AE signals, the subsequent macrocracking generates fewer signals of higher amplitude. As a result, the b-value progressively reduce its value when the damage in the specimen advance: this is the core of the so-called "b-value analysis" used for damage assessment.

On the other hand, the damage process is also characterized by a progressive localization identified through the fractal dimension D of the damaged domain. It may be proved that 2b=D (Aki, 1967; Carpinteri, 1994; Turcotte *et al.*, 2003). Therefore, by determining the b-value it becomes possible to identify the energy release modalities in a structural element during the AE monitoring process. In the extreme case D = 3.0, which corresponds to b=1.5, a critical condition in which the energy release takes place through small defects evenly distributed throughout the volume. For D=2.0, which corresponds to b = 1.0, the energy release takes place on a fracture surface. In the former case, diffused damage is observed, whereas in the latter case two dimensional cracks are formed leading to the separation of the structural specimen.

The similarity between AE monitoring in laboratory tests and seismic events is well explained by Scholz (1968). Scholz demonstrated that the statistical behavior of the micro-fracturing activity, observed in AE laboratory tests, is similar in many aspects to that observed in earthquakes and hence the same power law applies, as long as the signal trace amplitude measurements is obtained by means of AE devices, rather than seismograph instrumental magnitude measures.

3. LATTICE DISCRETE ELEMENT METHOD (LDEM)

The version of the truss-like Discrete Element Method (DEM) proposed by Riera (1984), which is used in this paper, is based on the representation of a solid of a cubic arrangement of elements which is only able to carry axial loads. The cubic module is presented in Figs. 1a and 1b. The mass is lumped at the nodes. Each node has three degrees of freedom, corresponding to the nodal displacements in the three orthogonal coordinate directions. The equations that relate the properties of the elements to the elastic constants for an isotropic medium are presented in Eq. (1).

$$\eta = \frac{9\nu}{4-8\nu},\ EA_n = E{L_c}^2\frac{(9+8\eta)}{2(9+12\eta)},\ EA_d = \frac{2\sqrt{3}}{3}A_n, \tag{1}$$

where E and ν denote Young's modulus and Poisson's ratio, respectively, while A_n and A_d are the areas of the normal and the diagonal elements and L_c is the size of the basic cubic module. The resulting motion equations obtained with this spatial discretization can be written in the well-known form presented in Eq. (2).

$$\mathbf{M}\ddot{\mathbf{x}}(t) + \mathbf{C}\dot{\mathbf{x}}(t) + \mathbf{F_r}(t) - \mathbf{P}(t) = 0, \tag{2}$$

where **x** is the vector of generalized nodal displacements, **M** is the diagonal mass matrix, **C** is the damping matrix, also assumed diagonal, $\mathbf{F_r}$ is the vector of the internal forces acting on the nodal masses and **P** is the vector of external forces. The operator $(\dot{\bullet})$ denotes the time (t) differentiation $d(\bullet)/dt$. If **M** and **C** are diagonal, the Eq. (2) is not coupled and, therefore, the explicit central finite difference scheme can be used to time domain integration. Since the nodal coordinates are updated for each time step, large displacements can be accounted in a natural and efficient manner. This article adopts a relationship between axial force and axial strain in the uniaxial elements (bar), based on the bilinear law proposed by Hillerborg (1978), which is presented in Fig. 1c. The specific fracture energy (*Gf*) is directly proportional to the area below the bilinear constitutive law. Another important feature of this approach is the assumption that *Gf* is a 3D random field with a Weibull probability distribution.

The local strain associated with maximum loading in each bar is called critical strain (ε_p). This value is also a random variable and its variability, which is measured using the coefficient of variation CV, is related to the *Gf* parameter by the Eq. (3),

$$CV_{\varepsilon_p} = 0.5CV_{G_f}. \tag{3}$$

The minimum value of ε_p, determined for each specimen bar, is associated with the global strain for which a specimen loses linearity.

Mesh perturbation was incorporated to improve the performance when the body is submitted to compression. At it is possible to observe in Fig. 1c, the bar failure occurs only when submitted to tensile solicitation. In compression, the bar have a linear elasticity behavior, see Iturrioz *et al.* (2013a).

More exhaustive explanations of this version of the lattice model can be found in Kosteski *et al.* (2011, 2012). Applications of the LDEM in studies involving non-homogeneous materials subjected to fracture, such as concrete and rock, can be found in Riera and Iturrioz (1998), Dalguer *et al.* (2003), Miguel *et al.* (2008), Iturrioz *et al.* (2009) and Miguel *et al.* (2010).

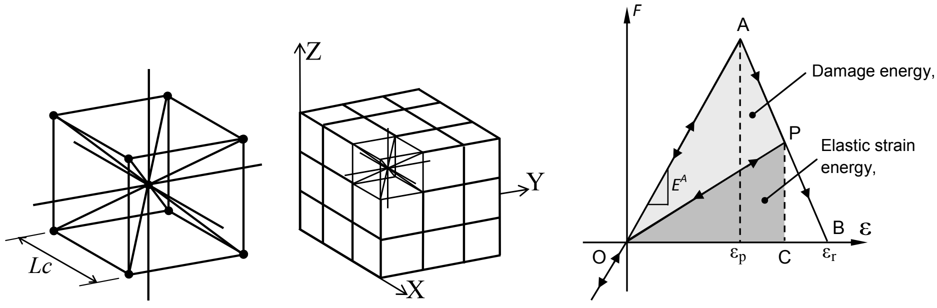

Figure 1. LDEM: (a) basic cubic module e (b) generation of a prismatic body and (c) Bilinear constitutive model with material damage.

4. APPLICATION

4.1 Model description

In the present work, three cubes are simulated considering standard concrete (quasi-fragile material) with different sizes (30, 60 and 90mm). The specimens are submitted to uniaxial compression, imposing a displacement in the vertical direction, with low velocity (the prescribed displacement does not induce dynamic effect during the simulation). Two sets of simulations are carried out with and without lateral restriction in both ends. Table 1 presents the input data adopted in the simulation. For all models, the same discretization level (the basic cubic module length (Lc) is 0.0025m) was used. Therefore, the three models with L=30mm, L=60mm and L=90mm were constructed with 12x12x12, 24x24x24 and 36x36x36 modules, respectively.

Table 1. Parameters adopted in the DEM simulations.

μ_{G_f}	CV_{G_f}	C_p	E	Rf_c	ρ	ν	Lc	L_{corr}
50 N/m	50%	2.5%	35 GPa	10.2 $\mathrm{m}^{-1/2}$	2400 $\mathrm{kg/m^3}$	0.25	0.0025 m	2xLc

The material toughness is defined as a random field characterized by the mean value μ_{G_f} and the variation coefficient CV_{G_f}, presented in Table 1, considering the Weibull statistical distribution defined as $W(G_f) = 1 - e^{-(G_f/\beta)^\gamma}$, where β and γ depend on μ_{G_f} and CV_{G_f}. This random field is also influenced by the correlation length (L_{corr}) which is assumed to be equal to 2xLc. The cubic module has an imperfection random field, using Gaussian distribution with mean zero and variation coefficient of C_p=2.5% of the Lc.

The other parameters, that define the model, are deterministic: the density (ρ), the initial Young's modulus (E), the Poisson's ratio (ν) and the failure factor (Rf_c). Equation (4) relates E, Rf_c and G_f to the critical strain, ε_p,

$$\varepsilon_p = Rf_c \sqrt{\frac{G_f}{E}}. \tag{4}$$

According to the constitutive law presented in Fig. 1c, the critical strain (ε_p) is defined where the max force occurs (point A).

4.2 Standard results

The main results are presented in this section. In Fig. 2 the results for global stress vs. global strain are presented for both boundary conditions (with and without lateral restrictions). These results are valid until the peak of the global stress-strain curve.

Figure 4a and Fig. 4b describe the two typical damage stages for quasi-fragile materials submitted to uniaxial compression. Initially, a global distribution of fissures in the same direction of the excitation appears due to the indirect tensile stress induced for the uniaxial compression. In the second stage, diagonal fissures appears and the energy dissipated by the friction between the inclined fissures becomes important (Gross and Seelig, 2011). This damage mechanism governs the post peak global curve. The stress peak decreases when the body length (L) increases, as presented in Fig. 2. These results characterize the size effect, which is intrinsic for quasi-fragile materials (see Rios and Riera, 2004).

The energy balance vs. the global strain for the case 60L (L=60mm without lateral restriction) is presented in Fig. 3a. It is possible to observe that a little quantity of energy (blue line) is dissipated by damage before reaching the load peak. In

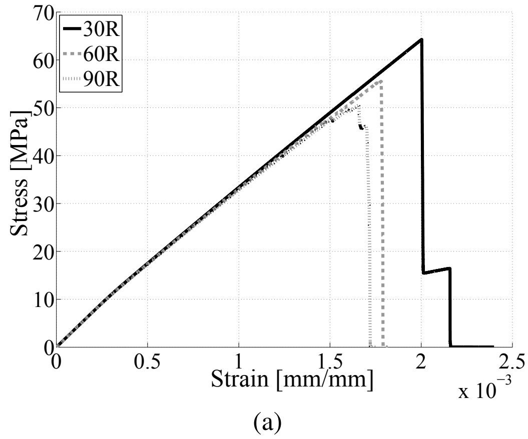

Figure 2. Global stress-strain curve for the three specimens analyzed: (a) with lateral restrictions in the ends and (b) without lateral restrictions in the ends.

Figure 3b, it is plotted the dissipated energy for bars oriented in the same load direction (black line) and normal to the load direction (red line). Bars which are perpendicular to the load direction (NBar) dissipate energy from low values of strain to the end of the process, and this dissipation is related to the first typical behavior in the damage process for the quasi-fragile specimens submitted to uniaxial compression (several microfissures are distributed in all domain due to indirect tensile stress, see Fig. 4a). Near the load peak, also it is presented in Fig. 3b, the energy dissipated by the bars aligned to the load (PBar) begin to increase when the fracture mode II appears and the friction becomes the main dissipation energy source (Fig. 4b illustrates this situation). This version of LDEM cannot capture the energy dissipation due to friction and therefore this work only considers the behavior up to the load peak. However, it should be mentioned that bending shear and uniaxial tensile damage processes can be represented through LDEM (pre and post load peak) using the same input data. Figure 3a and Fig. 3b present the global stress vs. strain curve (out of scale in light gray) and the zone where the LDEM results have no physical meaning (solid shadow area). Comparison between numerical and experimental results for concrete specimen submitted uniaxial load was presented in Iturrioz *et al.* (2014). In Rios and Riera (2004), Iturrioz *et al.* (2013a) and Miguel *et al.* (2008) presented numerical results and its comparison with experimental results.

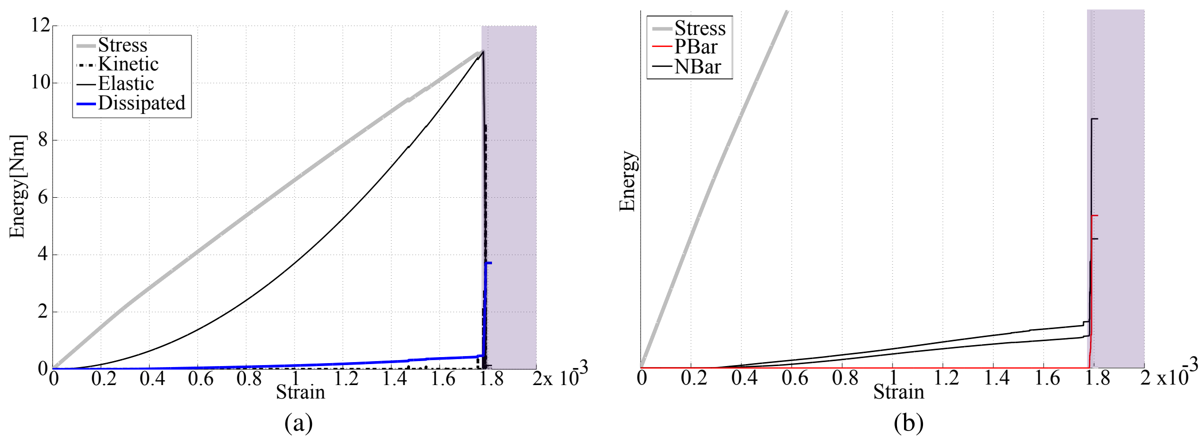

Figure 3. Curve that corresponds to the size L=60mm for the case without restriction in both ends (60L): (a) energy balance during the damage process and (b) dissipated energy for bars oriented in the same load direction (PBar) and normal to the load direction (NBar).

Final configuration results for specimen with L=90mm are presented in Figs. 5a, 5b and 5c for the case without lateral restriction in both ends (90L) and can be compared to the final experimental configuration in similar specimen presented in Fig. 4c. In Figs. 5d and 5e, two views for the case with lateral restriction in the ends (90R0 are presented. In Fig. 5f, two experimental configurations of similar specimen for lateral restriction in both ends are presented for comparison. In Fig. 5, red, orange and gray colors represent broken, damaged and undamaged bars, respectively. Comparing the experimental and numerical results, it is possible to see that the results are coherent, i.e., the same final fracture mechanism clearly appears.

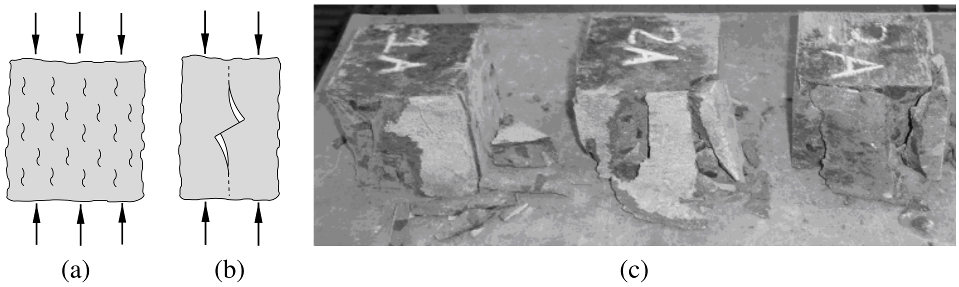

Figure 4. Schemes that illustrate the damage process in quasi-brittle materials under compression: (a) fissures appear in loading direction, (b) self-organization and propagation at an angle and the sliding dissipation process begins to be dominant. (c) Experimental results for the case without lateral restriction in both ends.

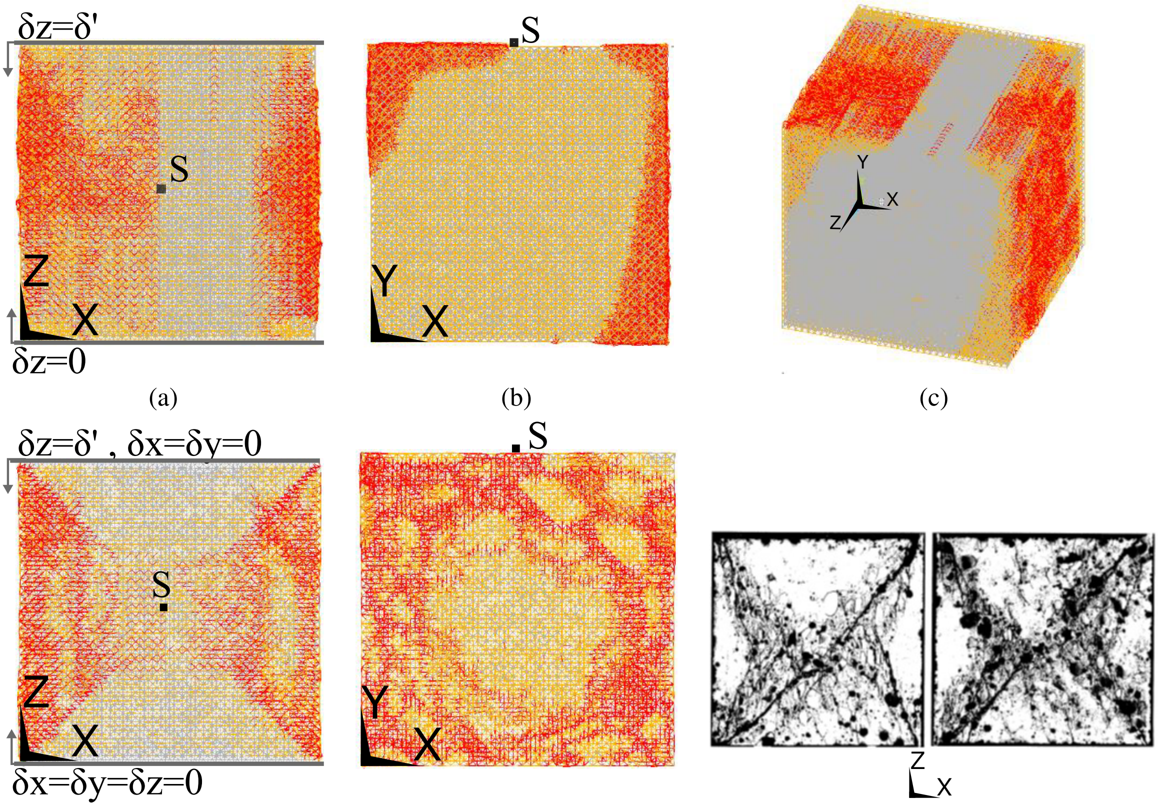

Figure 5. The final configuration for 90L (a, b and c) and 90R (d and e) models, where (a) and (d) illustrate the boundary conditions in each simulation. In (f), it is presented an experimental result with lateral restriction in the ends.

4.3 AE results

Acoustic emission signal for the simulated cases are presented in this section. In Figures 5a and 5d, the position (S) in the surface specimen where the acceleration is registered (simulating an AE device) are indicated. The acceleration was measured in a perpendicular direction to the surface position.

Comparison between experimental and numerical AE event amplitude (A) was carried out in both time (t) and frequency (f) domains, as can be see in Figure 6. One can notice that the results in the time and the frequency domain are similar.

In Figure 7a, accumulated ($Nacum$) and instantaneous number (N) of AE events are presented versus the normalized time. Another point for the latter information is presented in Fig. 7b, where the M value is defined as the logarithm of the AE amplitude. A comparison between cases without (60L) and with lateral restriction (60R) in the ends is presented in both figures. One can notice for the 60L case, there are no AE events between 0.3 to 0.7 of normalized time. In both cases

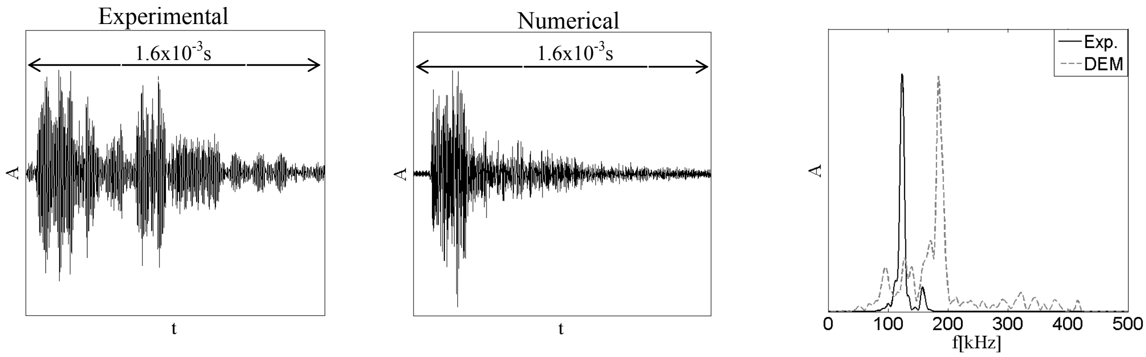

(a) (b)

Figure 6. Experimental and numerical comparison: (a) amplitude (A) vs. time (t); (b) amplitude (A) vs. frequency (f) for the three point bending test. (Iturrioz *et al.*, 2013b)

there is a great quantity of low AE events in the beginning and then the number and the amplitude of the events increases in the end of the simulation. The global stress curve was included (out of scale) in these figures.

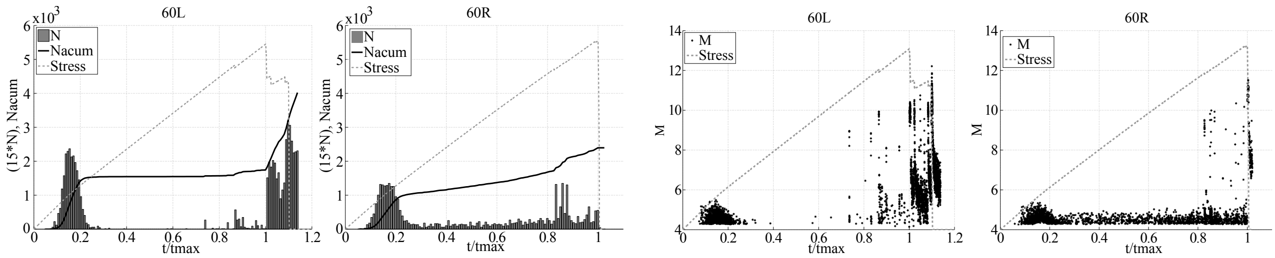

(a) (b)

Figure 7. Results for the specimen L=60mm with and without lateral restriction: (a) Accumulated and instantaneous numbers of AE events vs. normalized time. (b) M=log (AE amplitude) vs. normalized time. In all plots the global stress vs. normalized time out of scale are presented.

The *b*-value, which is the angular coefficient in the relation between $log(Nacum < M)$ vs. $M(M = logA)$, can be evaluated through Fig. 8a for the initial stage of the damage process for the specimen 60R. It can be noticed that this curve presents a linear behavior. In Fig. 8b, it is presented typical results obtained in experimental test by Carpinteri *et al.* (2009), where the *b*-value is usually within the interval [1, 1.5].

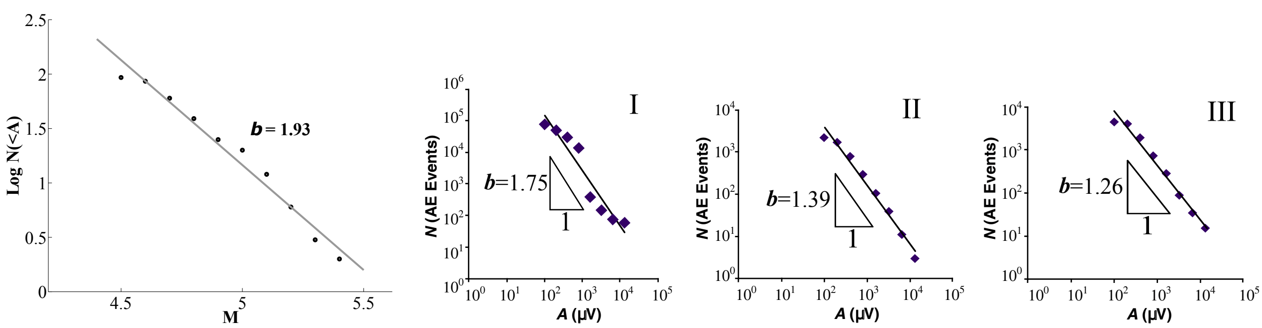

(a) (b)

Figure 8. Results in terms of *b*-value: (a) measured in the normalized time interval [0.4, 0.7] for the test 60L; (b) typical experimental result obtained in uniaxial test (Carpinteri *et al.*, 2009).

Finally, Fig. 9a presents the variation of *b* during all the process simulated for the specimen 60L (line with square dots) and the specimen 60R (line and circles). Figure 9b exposes three experimental curves for uniaxial compression tests carried out by Carpinteri *et al.* (2011). As indicated in section 2, it is possible to relate the dimension of the fissure distribution D to the *b* coefficient (D=2*b*).

Figure 9c presents the spatial distribution of the AE events sources in different intervals during the damage process. This result is interesting to compare different regions of the Fig. 9a with the position of the source of the AE during the simulation. The relation between these two figures are evident in the end of the 60L specimen, which occurs in the interval [0.80, 0.95] of normalized time. It can be observed that a low *b*-value (Fig. 9a) is related to AE events source that emanate from a located region (Fig. 9c) for case 60L[0.80, 0.95] and the case 60R[0.82, 0.85].

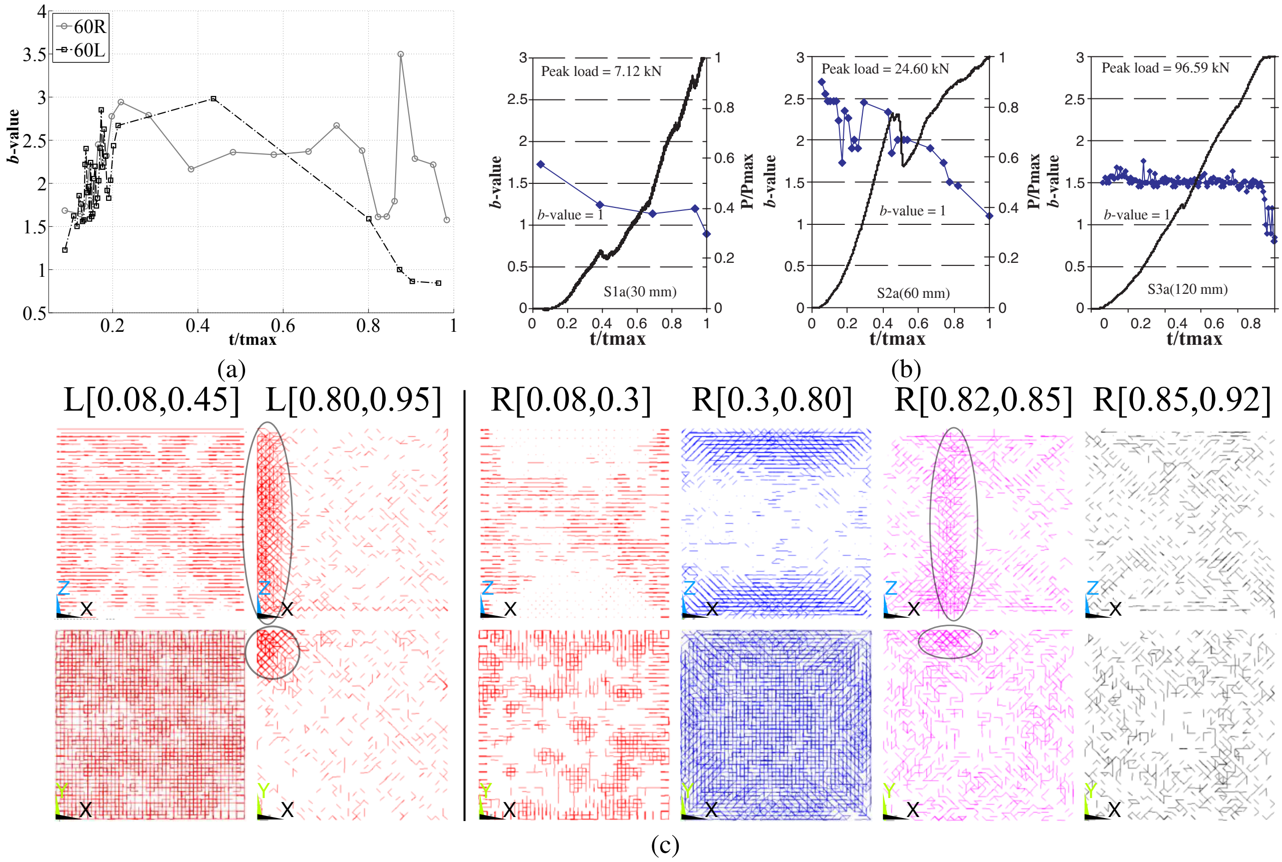

Figure 9. (a) The evolution of *b*-value during all the damage process; (b) Experimental results carried out by Carpinteri *et al.* (2011) in similar specimens; (c) the intervals and spatial distribution of the bars that produce the AE events during the damage process simulated.

5. CONCLUSIONS

In the present paper, the analyses of cubes submitted to compression are presented using a version of lattice discrete element method. Standard results in terms of global stress vs. strain, energy balance and final configuration are presented. Acoustic emission test results are also presented and discussed. Moreover, it is possible to conclude:

- The numerical method presented good performance in the simulation of the three cubes of concrete, until the stress peak;
- The size effect could be represented in terms of the maximum stress value computed in the specimens with different sizes and in terms of the final configuration;
- The results in terms of the acoustic emission simulation also help the understanding of the damage process.

6. ACKNOWLEDGEMENTS

The authors wish to thank the Brazilian agencies CNPq and Capes for funding this research.

7. REFERENCES

Aki, K., 1967. “Scaling law of seismic spectrum”. *Journal of Geophysical Research*, Vol. 72, No. 4, pp. 1217–1231.

Carpinteri, A., 1994. “Scaling laws and renormalization groups for strength and toughness of disordered materials”. *International Journal of Solids and Structures*, Vol. 31, No. 3, pp. 291–302.

Carpinteri, A., Lacidogna, G. and Manuello, A., 2011. "The b-value analysis for the stability investigation of the ancient athena temple in syracuse". *Strain*, Vol. 47, No. s1, pp. e243–e253.

Carpinteri, A., Lacidogna, G. and Niccolini, G., 2009. "Fractal analysis of damage detected in concrete structural elements under loading". *Chaos, Solitons & Fractals*, Vol. 42, No. 4, pp. 2047–2056.

Dalguer, L., Irikura, K. and Riera, J., 2003. "Simulation of tensile crack generation by three-dimensional dynamic shear rupture propagation during an earthquake". *Journal of Geophysical Research: Solid Earth (1978–2012)*, Vol. 108, No. B3.

Gross, D. and Seelig, T., 2011. *Fracture mechanics: with an introduction to micromechanics*. Springer Science & Business Media.

Hillerborg, A., 1978. "A model for fracture analysis". *Report TVBM-3005*.

Iturrioz, I., Lacidogna, G. and Carpinteri, A., 2013a. "Experimental analysis and truss-like discrete element model simulation of concrete specimens under uniaxial compression". *Engineering Fracture Mechanics*, Vol. 110, pp. 81–98.

Iturrioz, I., Lacidogna, G. and Carpinteri, A., 2013b. "Acoustic emission detection in concrete specimens: Experimental analysis and lattice model simulations". *International Journal of Damage Mechanics*. doi: 10.1177/1056789513494232.

Iturrioz, I., Riera, J. and Miguel, L., 2014. "Introduction of imperfections in the cubic mesh of the truss-like discrete element method". *Fatigue & Fracture of Engineering Materials & Structures*, Vol. 37, No. 5, pp. 539–552.

Iturrioz, I., Miguel, L.F.F. and Riera, J.D., 2009. "Dynamic fracture analysis of concrete or rock plates by means of the discrete element method". *Latin American Journal of Solids and Structures*, Vol. 6, No. 3, pp. 229–245.

Kosteski, L., D'Ambra, R.B. and Iturrioz, I., 2012. "Crack propagation in elastic solids using the truss-like discrete element method". *International journal of fracture*, Vol. 174, No. 2, pp. 139–161.

Kosteski, L., Iturrioz, I., Batista, R.G. and Cisilino, A.P., 2011. "The truss-like discrete element method in fracture and damage mechanics". *Engineering Computations*, Vol. 28, No. 6, pp. 765–787.

Krajcinovic, D., 1996. *Damage mechanics*, Vol. 41. Elsevier, Amsterdam.

Lemaitre, J. and Chaboche, J.L., 1990. *Mechanics of solid materials*. Cambridge: University Press.

Miguel, L.F.F., Iturrioz, I. and Riera, J.D., 2010. "Size effects and mesh independence in dynamic fracture analysis of brittle materials". *Computer Modeling in Engineering & Sciences(CMES)*, Vol. 56, No. 1, pp. 1–16.

Miguel, L.F.F., Riera, J.D. and Iturrioz, I., 2008. "Influence of size on the constitutive equations of concrete or rock dowels". *International Journal for Numerical and Analytical Methods in Geomechanics*, Vol. 32, No. 15, pp. 1857–1881.

Munjiza, A., 2009. "Special issue on the discrete element method: aspects of recent developments in computational mechanics of discontinua". *Engineering Computations*, Vol. 26, No. 6.

Riera, J. and Iturrioz, I., 1998. "Discrete elements model for evaluating impact and impulsive response of reinforced concrete plates and shells subjected to impulsive loading". *Nuclear Engineering and Design*, Vol. 179, No. 2, pp. 135–144.

Riera, J.D., 1984. "Local effects in impact problems on concrete structures". In *Proceedings of the Conference on Structural Analysis and Design of Nuclear Power Plants*. Porto Alegre, Brazil, Vol. 3.

Rios, R.D. and Riera, J.D., 2004. "Size effects in the analysis of reinforced concrete structures". *Engineering Structures*, Vol. 26, No. 8, pp. 1115–1125.

Scholz, C., 1968. "The frequency-magnitude relation of microfracturing in rock and its relation to earthquakes". *Bulletin of the Seismological Society of America*, Vol. 58, No. 1, pp. 399–415.

Turcotte, D.L., Newman, W.I. and Shcherbakov, R., 2003. "Micro and macroscopic models of rock fracture". *Geophysical Journal International*, Vol. 152, No. 3, pp. 718–728.

8. RESPONSIBILITY NOTICE

The authors are the only responsible for the printed material included in this paper.